Is Iterative Reconstruction an Alternative to Filtered Backprojection in Routine Processing of Dopamine Transporter SPECT Studies?

Walter Koch, MD[1]; Christine Hamann, MD[2]; Julia Welsch, MD[1]; Gabriele Pöpperl, MD[1]; Perry E. Radau, PhD[3]; and Klaus Tatsch, MD[1]

[1]*Department of Nuclear Medicine, University of Munich, Munich, Germany;* [2]*Department of Neurology, University of Munich, Munich, Germany; and* [3]*Department of Medical Biophysics, Sunnybrook & Women's College of Health Sciences, Toronto, Ontario, Canada*

In general, striatal dopamine transporter (DAT) binding is assessed by use of data reconstructed by filtered backprojection (FBP). The aim of this study was to investigate whether the use of an iterative reconstruction algorithm (ordered-subset expectation maximization [OSEM]) may provide results comparable to or even better than those obtained by standard FBP. **Methods:** In 50 patients with parkinsonian syndromes, SPECT scans were acquired 4 h after injection of 185 MBq of ^{123}I-fluoropropyl-2β-carbomethoxy-3β-(4-iodophenyl)tropane (^{123}I-FP-CIT) by use of a triple-head γ-camera fitted with low-energy, high-resolution fanbeam collimators. After reconstruction by FBP and OSEM, data were filtered with a Butterworth filter and corrected for attenuation. Patient studies were automatically fitted to a mean template with a corresponding 3-dimensional (3D) volume-of-interest map covering the striatum, caudate, and putamen as well as an occipital reference region to calculate specific DAT binding. In addition, studies with an anthropomorphic 3D striatal phantom were performed to mimic different pathologies. **Results:** Visual assessment of phantom and patient data suggested a better separation between the caudate and the putamen in studies reconstructed by OSEM than in those reconstructed by FBP. There was an excellent correlation between specific DAT binding assessed by OSEM and that assessed by FBP (R^2 values: striatum, 0.999; caudate, 0.998; putamen, 0.998). Mean specific striatal binding obtained by OSEM was approximately 6% lower than that obtained by FBP. In no case was diagnostic information from OSEM inferior to that from FBP. **Conclusion:** Iterative reconstruction of ^{123}I-FP-CIT SPECT studies for the assessment of DAT is feasible in routine clinical practice. A close correlation between FBP and OSEM data suggested that the latter also allow reliable quantification of DAT binding. Because of a better separation between the caudate and the putamen in the visual evaluation, as suggested by phantom and patient studies, OSEM may even be considered the preferable approach.

Key Words: iterative reconstruction; ^{123}I-FP-CIT; automatic data processing; dopamine transporter

J Nucl Med 2005; 46:1804–1811

Imaging of the presynaptic dopamine transporter (DAT) has evolved to be an important diagnostic tool in patients with parkinsonian syndromes (*1*). DAT SPECT studies can confirm or exclude the diagnosis of a neurodegenerative parkinsonian syndrome (*2*) and, in combination with semiquantification (*3*), can detect subtle changes in DAT binding in striatal subregions and allow monitoring of disease progression (*4,5*).

All common SPECT camera software packages allow image reconstruction by filtered backprojection (FBP), an algorithm well established for ^{123}I-fluoropropyl-2β-carbomethoxy-3β-(4-iodophenyl)tropane (^{123}I-FP-CIT) SPECT. Its most important benefit is rapid processing speed. However, some artifacts can be caused by the algorithm.

More recently, reconstruction models based on a different mathematic approach were developed and proposed as alternatives for filtered backprojection in heart (*6*), bone (*7*), and brain perfusion (*8*) SPECT. However, because of its anatomically small structures, imaging of the dopaminergic system needs special attention to optimize imaging conditions. Besides visual assessment, semiquantitative evaluation of radiotracer binding plays an essential role. It allows comparison of a single patient scan to normal reference values and enables follow-up investigations to monitor disease progression and therapeutic effects. Little is known about the use of iterative reconstruction techniques in neurotransmitter and neuroreceptor imaging with SPECT. Even though a previous study addressed this issue with phantom measurements (*9*), data in a large clinical context have not been published. Whether results obtained by different reconstruction algorithms can be compared directly and whether iterative reconstruction techniques allow accurate semiquantification for brain DAT scans remain to be proven.

In this study we evaluated the use of the iterative reconstruction algorithm ordered-subset expectation maximization (OSEM) in DAT SPECT studies assessed in a phantom and in patients, with the aim of comparing the results of reconstructions by OSEM with those by FBP.

Received May 20, 2005; revision accepted Aug. 11, 2005.

For correspondence contact: Walter Koch, MD, Department of Nuclear Medicine, University of Munich, Marchioninistrasse 15, 81377 Munich, Germany.

E-mail: walter.koch@med.uni-muenchen.de

MATERIALS AND METHODS

Patients

Fifty consecutive patients (ages: range, 36–78 y, mean ± SD, 62 ± 11 y) clinically presenting with parkinsonian syndromes were included in this retrospective data analysis. The patients were referred for routine clinical ^{123}I-FP-CIT SPECT investigations to establish or exclude the diagnosis of a neurodegenerative parkinsonian syndrome. Thus, a broad spectrum ranging from normal findings to severely decreased DAT binding was included.

Phantom

Phantom measurements were performed with the anthropomorphic basal ganglion phantom commercially available from Radiology Support Devices Inc. The phantom consists of symmetric chambers for each caudate (4.8 mL) and each putamen (6.0 mL) and a large chamber simulating the remaining brain (1,290 mL), all shaped according to the anatomy of the human brain. The chambers are surrounded by an artificial skull and soft tissue with attenuation coefficients equivalent to those of human tissue.

Measurements were performed with 11 activity concentrations of ^{123}I (ranging from 44.6 to 477.1 kBq/mL), each resulting in a different specific ratio between the striatum and the background region (27.9 kBq/mL). On the basis of previous phantom measurements, true specific ratios ranging from 0.6 to 16.1 were chosen to encompass the range known from routine SPECT studies of the dopaminergic system with ^{123}I-FP-CIT, covering the full range from markedly decreased radiotracer binding up to highly normal results, with some ratios being even higher than those observed in patient studies.

For the first phantom acquisition, the right striatal chambers (caudate and putamen chambers) were filled with the solution with the lowest ^{123}I concentration, and the left chambers were filled with the solution with the next higher activity concentration. For the following acquisitions, the striatal chambers were emptied, flushed, and then refilled with the next pair of concentrations. The large chamber simulating the brain with the exclusion of the basal ganglia (background) remained unchanged during the whole experiment. To minimize the adhesion of ^{123}I to the plastic chamber walls, a sodium iodine solution of 0.1 mol/L was used as the basis for all solutions.

To determine the true ratios achieved for the phantom, 2 separate 200-μL samples were taken from each chamber, and the activity concentrations in the samples were measured in a well counter (energy window, 140–220 keV; counting time, 1 min). The average counts per milliliter in each of the 2 identical samples were used to determine the ratios with the same formula as that used for clinical SPECT images.

SPECT Acquisition

Patients and the phantom were imaged under identical conditions. Data were acquired by use of a triple-head γ-camera (Picker Prism 3000; Philips) fitted with low-energy, high-resolution fanbeam collimators (focal distance, 530 mm). In patients, acquisition was started exactly 4 h after intravenous injection of 185 MBq of the radiopharmaceutical ^{123}I-FP-CIT (GE Healthcare). A 128 × 128 matrix was used for all acquisitions. The rotational radius was minimized and in the narrow range from 12.7 to 13.3 cm in all cases. A total of 120 projections were acquired at 60 s per view for patients, resulting in a total scan time of 43 min, and 15 s per view for the phantom with the camera heads following a circular orbit. Total brain counts of $>3 \times 10^6$ were achieved in all examinations. The projection data for the patient scans were checked visually for patient motion by use of the cine display and sinograms.

SPECT Processing

SPECT data were reconstructed with the FBP algorithm by use of a ramp filter with Odyssey-FX software (Philips), filtered with a Butterworth 3-dimensional (3D) postprocessing filter (0.60 cycle per centimeter, fifth order), and corrected for attenuation according to the Chang method (uniform loss, 0.11/cm; elliptic fitting with a separate contour for each slice (*3*)).

The iterative reconstruction was performed on a Hermes workstation (Nuclear Diagnostics) with the Hermes OSEM (HOSEM) program (OSEM implementation based on the algorithm of Richard Larkin, Macquarie University (*10*)). Three iterations, 8 subsets, a constant point spread function of 4 mm, and no background threshold were chosen. The radius of rotation was adjusted to account for the fanbeam geometry. The data were corrected for attenuation on the basis of manual elliptic fitting with a separate contour for each slice. As for the studies processed by FBP, a uniform loss of 0.11/cm was assumed. The established postreconstruction filtering parameters could not simply be transferred from FBP to OSEM. The resulting filtered images were too smooth, hampering precise anatomic mapping of the striatal structures (Fig. 1) and requiring adjustment of the cutoff empirically. For this purpose, selected phantom and patient scans were filtered with different settings, and optimized parameters were chosen from the visual impression of the reconstructed transverse images. An acceptable compromise between smoothing and noise for optimized

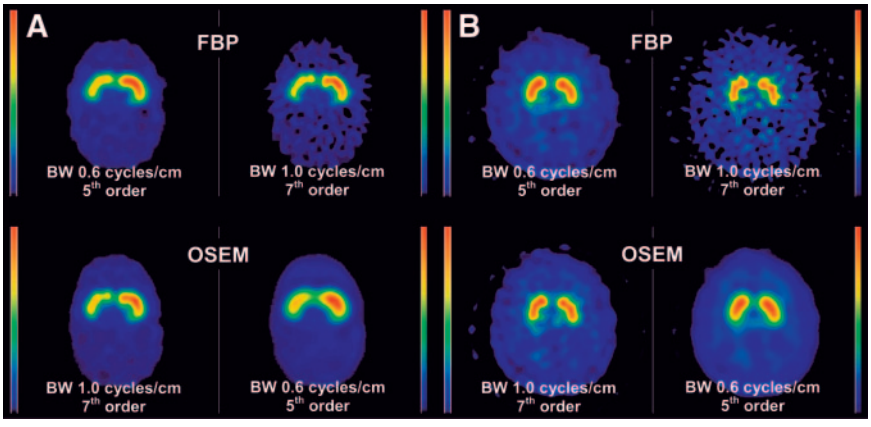

FIGURE 1. Influence of different cutoff frequencies of Butterworth (BW) filter on images reconstructed by OSEM and by FBP for scan of phantom (A) and scan of patient with normal DAT binding (B).

diagnostic image quality was obtained with a Butterworth 3D postprocessing filter (1.0 cycle per centimeter, seventh order).

Automated Semiquantitative Evaluation

The studies reconstructed with the OSEM algorithm were first coregistered to the images obtained by the FBP algorithm by use of the count difference registration algorithm in MultiModality software (Hermes; Nuclear Diagnostics). This procedure is necessary because the HOSEM software models the transverse angle rotational adjustment during the placement of the attenuation correction ellipses into the reconstructed data.

For patient and phantom SPECT scans, a modified version of brain analysis software (BRASS, version 3.4.4; Nuclear Diagnostics) running on a Hermes workstation was used for a standardized and observer-independent evaluation as published previously (*11*). Studies were registered to a template (based on studies reconstructed by FBP); subsequently, a standardized 3D voxel-of-interest (VOI) map was applied.

After registration of each FBP scan, the corresponding transformation matrix was applied in an identical manner to the coregistered study with iterative reconstruction to permit semiquantitative evaluation by use of the identically positioned VOI map.

The phantom studies were processed in an identical way. However, to gain full accuracy in the phantom scans, a special phantom template was created. For this purpose, images of the first SPECT measurement were coregistered to a CT scan of the phantom. The coregistered image was adjusted to 2.0-mm isotropic voxel dimensions and served as a template for the remaining studies. On the basis of the CT scan of the phantom, a 3D VOI map with regions for each striatum (1,409 voxels each) and a large occipital background region (8,624 voxels) in the remaining brain was drawn. The sizes and shapes of all VOIs were comparable to those of the standardized template used for the patient studies (striatum, 1,409 voxels; caudate, 524 voxels; putamen, 689 voxels; occipital reference, 8,588 voxels) (Fig. 2).

Comparison of Semiquantitative Results

The semiquantitative results were compared for the reconstruction techniques. For this purpose, the specific radiotracer binding ratios of the striatum, caudate, and putamen were calculated from the mean counts per voxel with the occipital cortex serving as a reference (specific binding in the striatum = [value for the striatum − value for the occipital cortex reference]/value for the occipital cortex reference). Because the underlying disease in patients with parkinsonian syndromes often affects the caudate and the putamen with different severities, the ratio of the specific binding in the putamen to that in the caudate also was calculated.

Image Quality

To assess the quality of images obtained by the reconstruction methods, all 50 scans were rated visually by 3 independent observers. For this purpose, a program was written to present the scans reconstructed by FBP and by the iterative algorithm for each patient side by side, in random order and unlabeled. Because the OSEM algorithm lacks the typical streak reconstruction artifacts known to appear outside the brain with FBP, it would have been easy to visually distinguish between the images. So that the study would be masked, all scans were presented to the observers with 2 different intensity threshold values: 30% to assess the striatal structures and 10% to rate brain areas with nonspecific binding. The observers were asked to answer 3 questions: "Which image shows the best delineation of the striatum?", "Which image allows the best differentiation between the caudate and the putamen?", and "Which image shows the most homogeneity of the areas with nonspecific binding?". They were also permitted to state that there was no visual difference between the images.

To objectively evaluate the homogeneity between the OSEM- and FBP-reconstructed images, histograms of the counts per voxel within the occipital reference region expressed as a percentage of the mean counts per voxel were plotted exemplarily for a phantom scan with different filter parameters.

Time Required for Processing of Individual Studies

The time needed to entirely process a subset of 10 randomly selected patients with both methods was recorded. For the OSEM reconstruction, the processing time on the computer system (Hermes workstation with a 1.8-GHz Pentium 4 processor and 512 MB of RAM), including manual placement of attenuation correc-

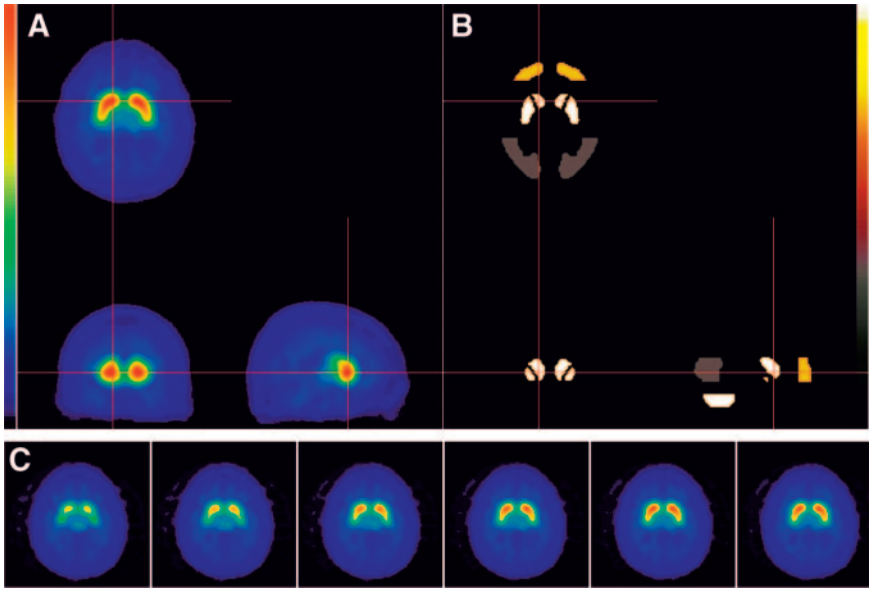

FIGURE 2. Mean template for healthy controls (A and C) and corresponding 3D VOI map (B) for semiquantitative evaluation.

TABLE 1
Results of Visual Assessment by 3 Independent Observers of Studies Reconstructed with FBP and with OSEM

	No. of scans (n = 50) showing:								
	Better delineation of striatum			Better differentiation of caudate and putamen			More homogeneous nonspecific binding		
Observer	OSEM	FBP	NV	OSEM	FBP	NV	OSEM	FBP	NV
1	49	1	0	22	1	27	50	0	0
2	37	2	11	20	1	29	49	1	0
3	44	2	4	19	0	31	49	1	0

NV = no visual difference between FBP and OSEM.

tion ellipses, was recorded. For the FBP reconstruction, the corresponding time was recorded on the Odyssey FX computer.

Statistics

Correlations between semiquantitative results of studies reconstructed by both reconstruction algorithms were calculated by linear regression analyses. For the regression analyses, the right and the left striatal regions were included as separate datasets. To quantify the accuracy of the regression curves, the R^2 values and SEs of the slopes were determined. To further estimate the range of deviations expected when the FBP reconstruction method was replaced by the OSEM algorithm, the difference between the semiquantitative results of both methods averaged over all scans ($\bar{d}$), the corresponding SD (s), and the limits of agreement ($\bar{d} - 2s$ and $\bar{d} + 2s$) were calculated as proposed by Bland and Altman (*12*). In addition, intraclass correlation coefficients (ICC) based on a 2-way random model were determined, and a variation index was defined as used for test-retest variation testing by Seibyl et al. (*13*): variation index (%) = [absolute(FBP ratio − OSEM ratio) × 200%]/(FBP ratio + OSEM ratio).

Because the binding ratios evaluated by the iterative reconstruction method were lower than those obtained by the FBP reconstruction method (as shown by a linear regression slope lower than that of the line of equality), the semiquantitative results evaluated by use of images with iterative reconstruction had to be corrected to be directly comparable to those obtained by FBP reconstruction and to calculate statistics. For this purpose, all binding ratios were multiplied by the reciprocal slope of the regression curve.

In the phantom model, the semiquantitative results obtained from images reconstructed by the OSEM algorithm were also compared with the true ratios in the phantom determined by well counter measurements.

All statistical analyses were performed with SPSS software (SPSS Inc.).

RESULTS

Assessment of Image Quality

The results of the independent visual readings of all 50 patient scans by 3 observers are listed in Table 1. Figure 3 shows the effects of different filter parameters applied to FBP-reconstructed images on the delineation of the striatal structures and the homogeneity of the areas with nonspecific binding in comparison with an OSEM-reconstructed image with visually optimized filter parameters for a phantom scan.

Comparison of Semiquantitative Results of Reconstruction Methods

The correlations between specific binding ratios evaluated from images reconstructed with the OSEM and FBP algorithms in patient studies are summarized in Table 2. Specific ratios calculated from the OSEM-reconstructed images were, on average, 6% lower than those calculated from the FBP-reconstructed images. After correction for this

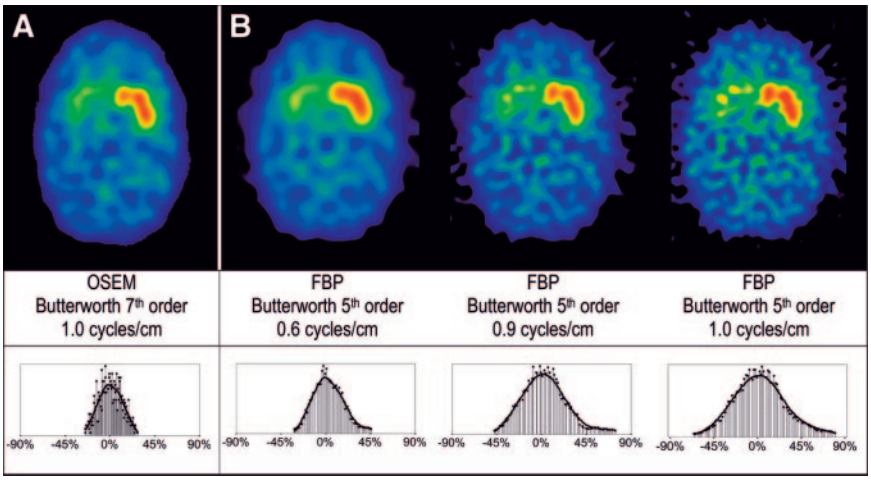

FIGURE 3. Example of differentiation between caudate and putamen in OSEM-reconstructed images (A) and in images reconstructed by FBP with various filter parameters (B) for phantom scan. Histograms show activity distribution within occipital reference region expressed as percent difference from mean counts per voxel.

TABLE 2
Parameters of Linear Regression for Specific Binding Ratios from OSEM- and FBP-Reconstructed Images

Scans	Parameter	Value for*: Striatum	Caudate	Putamen	Putamen-to-caudate ratio†
Phantom (n = 11‡)	R^2	0.998			
	Slope ± SE	0.88 ± 0.01			
	ICC	0.978			
Patient (n = 50)	R^2	0.999	0.998	0.998	0.996
	Slope ± SE	0.94 ± 0.00	0.94 ± 0.00	0.95 ± 0.00	1.01 ± 0.01
	ICC	0.985	0.970	0.991	0.978

*All correlations were statistically significant at $P < 0.001$.
†Ratio of specific binding in putamen to that in caudate.
‡n = number of different activity concentrations in phantom.

finding, the mean difference between the specific binding ratios calculated from the OSEM- and FBP-reconstructed images, the corresponding limits of agreement, and the variation indices were determined (Table 3). The results of the ICC analyses are in line with those obtained by the Bland–Altman algorithm.

The ratios of the specific binding in the putamen to that in the caudate, obtained by both methods of reconstruction, were almost identical, with a slope of the regression line of 1.01.

The corresponding data in the phantom studies are shown in Figure 4 and Table 2. The percent recovery, obtained by comparing measured specific ratios with true ratios in the phantom model, were 42% for the iterative reconstruction technique and 48% for the FBP reconstruction technique.

Comparison of Processing Times

The mean processing time for the reconstruction, filtering, and attenuation correction with the OSEM software (averaged for a subset of 10 patient studies) was 6 min per study. The same task for the FBP software took, on average, 6 min. For both reconstruction methods, the reconstruction time was shorter than the time required to manually place attenuation correction ellipses.

DISCUSSION

Numerous effects degrade image quality in DAT SPECT. Many of them have their origins in imaging physics, that is, tissue scatter and attenuation, statistical noise, depth dependence of the point spread function, collimator blurring, and restricted spatial and energy resolution. Low count statistics further aggravate reconstruction problems. Until now, studies of the dopaminergic system have been reconstructed mainly with the FBP algorithm, which is available on each SPECT device. The algorithm tries to compensate for statistical noise with a variety of filter techniques (e.g., ramp filter). However, the effectiveness is limited by coarse sampled data and leads to streak artifacts that are easily recognizable outside the scanned object but less easily recognizable within the object examined. In addition, FBP cannot account for the above-mentioned physical phenomena, resulting in a loss of resolution and of image contrast.

As an alternative, a variety of iterative reconstruction methods have been discussed in the literature (*14*). These include the simultaneous iterative reconstruction technique (*14*), the algebraic reconstruction technique (*15*), the maximum-likelihood expectation maximization algorithm (*16–18*), and the OSEM algorithm (*8,10,19–21*). These tech-

TABLE 3
Deviation Between Semiquantitative Measures of OSEM- and FBP-Reconstructed Images

Scans	Parameter	Value for: Striatum	Caudate	Putamen	Putamen-to-caudate ratio*
Phantom (n = 11†)	Mean difference ± SD	0.05 ± 0.17			
	Limits of agreement	−0.30 to +0.40			
	Variation index ± SD (%)	7.1 ± 5.3			
Patient (n = 50)	Mean difference ± SD	0.00 ± 0.06	0.00 ± 0.09	0.00 ± 0.06	0.00 ± 0.04
	Limits of agreement	−0.12 to +0.12	−0.19 to +0.19	−0.12 to +0.12	−0.08 to +0.08
	Variation index ± SD (%)	3.3 ± 2.7	4.3 ± 3.1	4.5 ± 3.5	5.1 ± 4.1

*Ratio of specific binding in putamen to that in caudate.
†n = number of different activity concentrations in phantom.

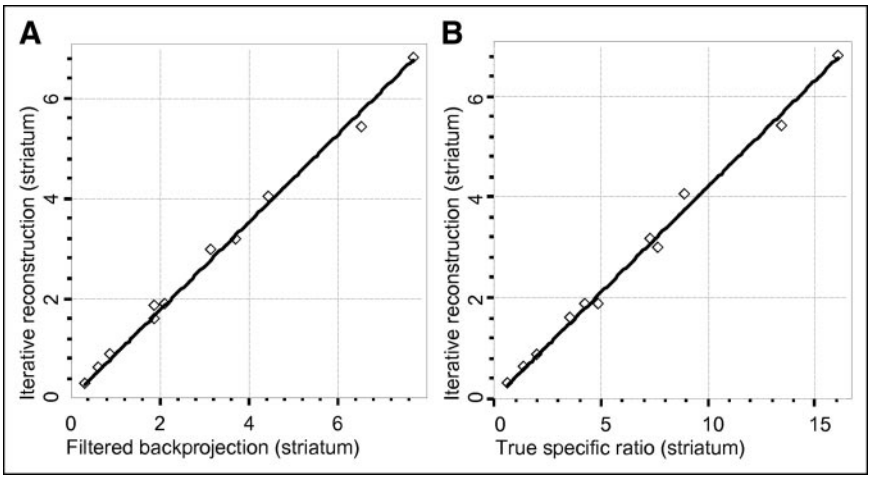

FIGURE 4. Correlation graphs of specific binding ratios obtained from images reconstructed by FBP and OSEM algorithms (A) in phantom model and correlation of OSEM-produced binding ratios with true activity ratios (B) for phantom. Corresponding regression line parameters are shown in Table 2.

niques are able to minimize attenuation artifacts, improve contrast and image resolution (*8,19*), and allow management of noise propagation with an abundance of regularization techniques. The process of iterative reconstruction can be described briefly by 4 essential steps: forward projection (simulated projections are calculated on the basis of the assumptions of the imaged object by simulating SPECT physics), comparison of measured and calculated projections, backprojection of the correction tendencies into the object volume, and a final correction step. These steps may be repeated several times to increase the reconstruction accuracy, explaining the excessive computational power demand of iterative reconstruction techniques and limiting their routine use in the past. Another drawback of the OSEM algorithm is its tendency to cause additional noise in reconstructed images when too many iteration steps are performed (*22*). The number of iterations and subsets has to be chosen empirically to optimize the image quality. With increasing processing power of computer systems and accelerated processing algorithms such as OSEM (*10*), the use of iterative reconstruction has become more widespread. However, there is still uncertainty about the impact of replacement of the reconstruction algorithm on critical imaging conditions, for example, those in DAT imaging.

In our study, the HOSEM software was used as camera-independent reconstruction software to reconstruct ^{123}I-FP-CIT SPECT scans.

The evaluation of the image quality of all 50 patient scans independently by 3 specialists in DAT SPECT showed promising results. None of the scans showed the streak artifacts known to appear with FBP, and all of the scans were considered suitable for routine reading. In almost all scans, the delineation of the striatal structures was improved in OSEM-reconstructed images, according to all 3 observers. Many scans allowed better distinction between the caudate and the putamen in patients with some activity preserved in the putamen. In nearly all of the OSEM-reconstructed images, there was more homogeneous nonspecific radiotracer accumulation in the occipital cortex, compared with the results obtained with FBP reconstruction. The clinical importance of this improved differentiation between the caudate and the putamen, however, remains unclear and will have to be further examined. In patients with early parkinsonian syndromes, a subtle loss of putamen binding might be more easily recognizable if the putamen is clearly distinguishable from the caudate. When manual semiquantification methods are used, detailed differentiation between the striatal subregions facilitates region-of-interest positioning and, as a result, might reduce inter- and intraobserver variabilities.

One could argue that the better differentiation between the caudate and the putamen in the OSEM-reconstructed images could be the result of the optimized filtering parameters. In fact, increasing the cutoff value for the FBP low-pass filter can enhance the distinction of striatal substructures in images reconstructed by FBP, as shown in Figure 3 for 1 of the phantom scans. However, this enhancement is limited by a rapid decrease in the homogeneity of the remaining brain in the phantom model, as depicted in the count statistic histograms of the occipital reference region. Whereas this phenomenon could be ignored in the occipital cortex, which serves mainly as a reference region for semiquantification, it also affects areas of interest (such as the opposite striatum in the phantom experiment), resulting in poor diagnostic image quality.

Two observers remarked that, despite the improved delineation of the striatal structures, the OSEM-reconstructed images looked different from the FBP-reconstructed images and attributed this finding to slightly lower contrast between striatal activity and nonspecific binding. This finding could be confirmed by the semiquantitative evaluation. An excellent linear correlation of semiquantitative results (high R^2 values and ICCs) could be shown for all regions with identical slopes of the regression lines, but the binding ratios obtained from OSEM studies were, on average, 6% lower than those obtained from FBP studies. Not only the different reconstruction algorithm but also the different filter parameters (*23*) most likely accounted for the lower semiquanti-

tative results, because filter parameters were chosen to provide optimized diagnostic image quality and not to maximize specific striatal binding ratios. The contours and method of attenuation correction have comparatively minor impacts on the semiquantitative results. Slightly lower binding ratios likely will not influence the diagnostic accuracy of ^{123}I-FP-CIT imaging with high ratios of specific binding to nonspecific binding; however, reference values need to be adjusted when the reconstruction method in routine clinical use is changed. The ratios of the specific binding in the putamen to that in the caudate were directly comparable between FBP and OSEM, because the counts per voxel in the subregions of the caudate and the putamen were reduced by the same factor. The visually improved delineation of the caudate and the putamen also did not change the ratio of the specific binding in the putamen to that in the caudate.

After correction of the specific binding ratios of the OSEM-reconstructed images for the different regression slopes, the OSEM-reconstructed images delivered striatal binding ratios in the narrow range of 0.1 below to 0.1 above those measured from FBP-reconstructed images. In the smaller caudate subregion, the range of deviations was only marginally higher. Because the literature reports considerably larger differences in specific binding between patients with and patients without neurodegeneration (average DAT binding loss of 57% in the putamen, as shown by Tissingh et al. (*24*)), the observed range of differences likely will not lower the diagnostic power. In addition, the variation index of the semiquantitative measures of both methods (3%) was lower than the variability range of repeated scans observed in test-retest studies (*13,25,26*). Much of this variation likely can be explained by the inherent intra- and interoperator variabilities of ellipse fitting for the attenuation correction process. An influence of VOI placement can be ruled out entirely, because realignment and VOI placement were performed automatically and are standardized for images from both reconstruction methods (identical transformation matrices). The BRASS software used for this purpose has been shown to be clinically useful (*11,27*). Furthermore, the software has been proven to be reliable, reproducible, and convenient (*27–30*).

One of the most challenging applications of DAT imaging is the use as a possible surrogate marker in research trials for monitoring disease progression and beneficial effects of potentially neuroprotective drugs (*4,5,31–33*). To accurately determine DAT loss over time, specific binding ratios should correlate linearly to true DAT density. Information about true radiotracer binding can be derived only from phantom studies. As shown in Figure 4, the correlation of the specific ratios obtained from OSEM-reconstructed images with the true ratios calculated from well counter measurements as a reference was linear in the full range of binding ratios observed in patient studies. The measured specific ratios were lower than the true ratios. This "recovery effect" was described previously, with similar values being reported (*34,35*). Scatter, absorption, and partial-volume effects (spatial resolution, region of interest, and lesion size) are responsible factors (*36*).

Solutions for scatter (*8,21,36,37*) and partial-volume effects (*38*) have been described, but some of these methods require either extensive phantom measurements for calibration or the acquisition of additional scatter windows. When these corrections are applied, more accurate semiquantitative ratios can be obtained (*9*). Unfortunately, the technical requirements are often not met by commonly used camera software. In addition, these techniques are complicated to implement in routine clinical practice and thus are less practical for routine clinical examinations; therefore, they were omitted in our studies.

Our results are in line with the improved image quality obtained with iterative reconstruction in a study by Van Laere et al. (increased contrast and improved delineation between gray matter and white matter), who used phantom studies with ^{201}Tl, ^{153}Gd, and ^{99m}Tc (*39*). It has even been postulated that iterative reconstruction narrows the gap in image quality between SPECT and ^{18}F-fluoro-L-dopa PET studies (*40*).

CONCLUSION

The OSEM reconstruction algorithm is a valuable tool in routine clinical ^{123}I-FP-CIT SPECT scans of DAT. The method provides image quality superior to that provided by the FBP reconstruction algorithm, with improved delineation of the caudate and the putamen in many cases. The semiquantitative specific binding ratios showed an excellent correlation both with the ratios obtained from FBP reconstructions and (in the phantom model) with the true ratios within the scanned object.

REFERENCES

1. Booij J, Speelman JD, Horstink MW, Wolters EC. The clinical benefit of imaging striatal dopamine transporters with [^{123}I]FP-CIT SPET in differentiating patients with presynaptic parkinsonism from those with other forms of parkinsonism. *Eur J Nucl Med*. 2001;28:266–272.
2. Benamer TS, Patterson J, Grosset DG, et al. Accurate differentiation of parkinsonism and essential tremor using visual assessment of [^{123}I]-FP-CIT SPECT imaging: the [^{123}I]-FP-CIT study group. *Mov Disord*. 2000;15:503–510.
3. Tatsch K, Asenbaum S, Bartenstein P, et al. European Association of Nuclear Medicine procedure guidelines for brain neurotransmission SPET using (123)I-labelled dopamine transporter ligands. *Eur J Nucl Med Mol Imaging*. 2002;29: BP30–BP35.
4. Chouker M, Tatsch K, Linke R, Pogarell O, Hahn K, Schwarz J. Striatal dopamine transporter binding in early to moderately advanced Parkinson's disease: monitoring of disease progression over 2 years. *Nucl Med Commun*. 2001;22:721–725.
5. Pirker W, Djamshidian S, Asenbaum S, et al. Progression of dopaminergic degeneration in Parkinson's disease and atypical parkinsonism: a longitudinal beta-CIT SPECT study. *Mov Disord*. 2002;17:45–53.
6. Hatton RL, Hutton BF, Angelides S, Choong KK, Larcos G. Improved tolerance to missing data in myocardial perfusion SPET using OSEM reconstruction. *Eur J Nucl Med Mol Imaging*. 2004;31:857–861.
7. Starck SA, Ohlsson J, Carlsson S. An evaluation of reconstruction techniques and scatter correction in bone SPECT of the spine. *Nucl Med Commun*. 2003;24: 565–570.
8. Kauppinen T, Koskinen MO, Alenius S, Vanninen E, Kuikka JT. Improvement of brain perfusion SPET using iterative reconstruction with scatter and non-uniform attenuation correction. *Eur J Nucl Med*. 2000;27:1380–1386.
9. Pareto D, Cot A, Pavia J, et al. Iterative reconstruction with correction of the

spatially variant fan-beam collimator response in neurotransmission SPET imaging. *Eur J Nucl Med Mol Imaging*. 2003;30:1322–1329.
10. Hudson H, Larkin R. Accelerated image reconstruction using ordered subsets of projection data. *IEEE Trans Med Imaging*. 1994;13:594–600.
11. Koch W, Radau P, Hamann C, Tatsch K. Clinical testing of an optimized software solution for an automated, observer-independent evaluation of dopamine transporter SPECT studies. *J Nucl Med*. 2005;46:1109–1118.
12. Bland JM, Altman DG. Statistical methods for assessing agreement between two methods of clinical measurement. *Lancet*. 1986;1:307–310.
13. Seibyl JP, Marek K, Sheff K, et al. Test/retest reproducibility of iodine-123-betaCIT SPECT brain measurement of dopamine transporters in Parkinson's patients. *J Nucl Med*. 1997;38:1453–1459.
14. Gilbert P. Iterative methods for the three-dimensional reconstruction of an object from projections. *J Theor Biol*. 1972;36:105–117.
15. Gordon R, Bender R, Herman GT. Algebraic reconstruction techniques (ART) for three-dimensional electron microscopy and x-ray photography. *J Theor Biol*. 1970;29:471–481.
16. Shepp L, Vardi Y. Maximum likelihood reconstruction for emission tomography. *IEEE Trans Med Imaging*. 1982;1:113–122.
17. Nuyts J, Dupont P, Stroobants S, Maes A, Mortelmans L, Suetens P. Evaluation of maximum likelihood based attenuation correction in positron emission tomography. *IEEE Trans Nucl Sci*. 1999;46:1136–1141.
18. Lange K, Carson R. EM reconstruction algorithms for emission and transmission tomography. *J Comput Assist Tomogr*. 1984;8:306–316.
19. Kauppinen T, Yang J, Kilpelainen H, Kuikka JT. Quantitation of neuroreceptors: a need for better SPECT imaging. *Nuklearmedizin*. 2001;40:102–106.
20. Pretorius PH, King MA, Pan TS, de Vries DJ, Glick SJ, Byrne CL. Reducing the influence of the partial volume effect on SPECT activity quantitation with 3D modelling of spatial resolution in iterative reconstruction. *Phys Med Biol*. 1998; 43:407–420.
21. Beekman FJ, Kamphuis C, Frey EC. Scatter compensation methods in 3D iterative SPECT reconstruction: a simulation study. *Phys Med Biol*. 1997;42: 1619–1632.
22. Hutton BF, Hudson HM, Beekman FJ. A clinical perspective of accelerated statistical reconstruction. *Eur J Nucl Med*. 1997;24:797–808.
23. Sjorgreen K, Ljungberg M, Strand SE. Parameters influencing volume and activity quantitation in SPECT. *Acta Oncol*. 1996;35:323–330.
24. Tissingh G, Booij J, Bergmans P, et al. Iodine-123-*N*-omega-fluoropropyl-2β-carbomethoxy-3β-(4-iodophenyl)tropane SPECT in healthy controls and early-stage, drug-naive Parkinson's disease. *J Nucl Med*. 1998;39:1143–1148.
25. Booij J, Habraken JB, Bergmans P, et al. Imaging of dopamine transporters with iodine-123-FP-CIT SPECT in healthy controls and patients with Parkinson's disease. *J Nucl Med*. 1998;39:1879–1884.
26. Hwang WJ, Yao WJ, Wey SP, Ting G. Reproducibility of ^{99m}Tc-TRODAT-1 SPECT measurement of dopamine transporters in Parkinson's disease. *J Nucl Med*. 2004;45:207–213.
27. Van Laere KJ, Warwick J, Versijpt J, et al. Analysis of clinical brain SPECT data based on anatomic standardization and reference to normal data: an ROC-based comparison of visual, semiquantitative, and voxel-based methods. *J Nucl Med*. 2002;43:458–469.
28. Radau PE, Linke R, Slomka PJ, Tatsch K. Optimization of automated quantification of ^{123}I-IBZM uptake in the striatum applied to parkinsonism. *J Nucl Med*. 2000;41:220–227.
29. Radau PE, Slomka PJ, Julin P, Svensson L, Wahlund LO. Evaluation of linear registration algorithms for brain SPECT and the errors due to hypoperfusion lesions. *Med Phys*. 2001;28:1660–1668.
30. Slomka PJ, Radau P, Hurwitz GA, Dey D. Automated three-dimensional quantification of myocardial perfusion and brain SPECT. *Comput Med Imaging Graph*. 2001;25:153–164.
31. Parkinson Study Group. Dopamine transporter brain imaging to assess the effects of pramipexole vs levodopa on Parkinson disease progression. *JAMA*. 2002;287: 1653–1661.
32. Schwarz J, Storch A, Koch W, Pogarell O, Radau PE, Tatsch K. Loss of dopamine transporter binding in Parkinson's disease follows a single exponential rather than linear decline. *J Nucl Med*. 2004;45:1694–1697.
33. Pirker W, Holler I, Gerschlager W, Asenbaum S, Zettinig G, Brucke T. Measuring the rate of progression of Parkinson's disease over a 5-year period with beta-CIT SPECT. *Mov Disord*. 2003;18:1266–1272.
34. Hashimoto J, Sasaki T, Ogawa K, et al. Effects of scatter and attenuation correction on quantitative analysis of beta-CIT brain SPET. *Nucl Med Commun*. 1999;20:159–165.
35. Soret M, Koulibaly PM, Darcourt J, Hapdey S, Buvat I. Quantitative accuracy of dopaminergic neurotransmission imaging with ^{123}I SPECT. *J Nucl Med*. 2003; 44:1184–1193.
36. Geworski L, Knoop BO, de Cabrejas ML, Knapp WH, Munz DL. Recovery correction for quantitation in emission tomography: a feasibility study. *Eur J Nucl Med*. 2000;27:161–169.
37. Ichihara T, Ogawa K, Motomura N, Kubo A, Hashimoto S. Compton scatter compensation using the triple-energy window method for single- and dual-isotope SPECT. *J Nucl Med*. 1993;34:2216–2221.
38. El Fakhri G, Moore SC, Maksud P, Aurengo A, Kijewski MF. Absolute activity quantitation in simultaneous ^{123}I/^{99m}Tc brain SPECT. *J Nucl Med*. 2001;42:300–308.
39. Van Laere K, Koole M, Kauppinen T, Monsieurs M, Bouwens L, Dierck R. Nonuniform transmission in brain SPECT using ^{201}Tl, ^{153}Gd, and ^{99m}Tc static line sources: anthropomorphic dosimetry studies and influence on brain quantification. *J Nucl Med*. 2000;41:2051–2062.
40. Tatsch K. Can SPET imaging of dopamine uptake sites replace PET imaging in Parkinson's disease? *Eur J Nucl Med Mol Imaging*. 2002;29:711–714.